Article

Visible Light Excitable Zn Fluorescent Sensor Derived from an Intramolecular Charge Transfer Fluorophore and Its in Vitro and in Vivo Application

Fang Qian, Changli Zhang, Yumin Zhang, Weijiang He, Xiang Gao, Ping Hu, and Zijian Guo

J. Am. Chem. Soc., **2009**, 131 (4), 1460-1468 • DOI: 10.1021/ja806489y • Publication Date (Web): 12 January 2009

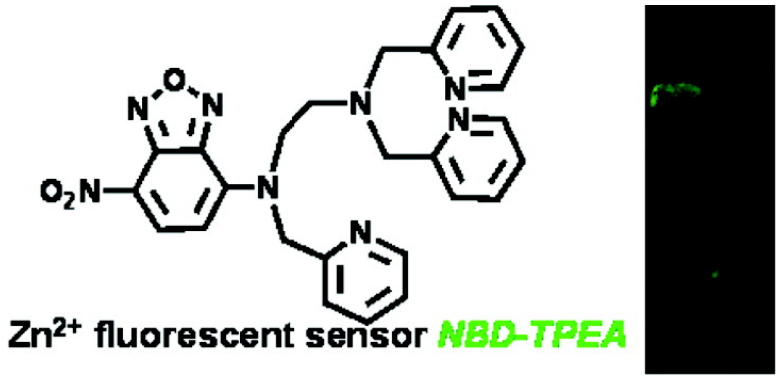

More About This Article

Additional resources and features associated with this article are available within the HTML version:

- Supporting Information
- Access to high resolution figures
- Links to articles and content related to this article
- Copyright permission to reproduce figures and/or text from this article

View the Full Text HTML

J|A|C|S ARTICLES

Published on Web 01/12/2009

Visible Light Excitable Zn^{2+} Fluorescent Sensor Derived from an Intramolecular Charge Transfer Fluorophore and Its in Vitro and in Vivo Application

Fang Qian,[†] Changli Zhang,[†,§] Yumin Zhang,[†] Weijiang He,*[,†] Xiang Gao,[‡] Ping Hu,[‡] and Zijian Guo*[,†]

State Key Laboratory of Coordination Chemistry, Coordination Chemistry Institute, School of Chemistry and Chemical Engineering, Nanjing University, Nanjing 210093, P. R. China, Animal Model Research Center, Nanjing University, Nanjing 210061, P. R. China, and Department of Chemistry, Nanjing Xiaozhuang College, Nanjing 210017, P. R. China

Received August 15, 2008; E-mail: zguo@nju.edu.cn; heweij69@nju.edu.cn

Abstract: The UV- and sensor-induced interferences to living systems pose a barrier for in vivo Zn^{2+} imaging. In this work, an intramolecular charge transfer (ICT) fluorophore of smaller aromatic plane, 4-amino-7-nitro-2,1,3-benzoxadiazole, was adopted to construct visible light excited fluorescent Zn^{2+} sensor, **NBD-TPEA**. This sensor demonstrates a visible ICT absorption band, a large Stokes shift, and biocompatibility. It emits weakly ($\Phi = 0.003$) without pH dependence at pH 7.1−10.1, and the λ_{ex} and λ_{em} are 469 ($\varepsilon_{469} = 2.1 \times 10^4$ M^{-1} cm^{-1}) and 550 nm, respectively. The **NBD-TPEA** displays distinct selective Zn^{2+}-amplified fluorescence ($\Phi = 0.046$, $\varepsilon_{469} = 1.4 \times 10^4$ M^{-1} cm^{-1}) with emission shift from 550 to 534 nm, which can be ascribed to the synergic Zn^{2+} coordination by the outer bis(pyridin-2-ylmethyl)amine (BPA) and 4-amine. The Zn^{2+} binding ratio of **NBD-TPEA** is 1:1. By comparison with its analogues **NBD-BPA** and **NBD-PMA**, which have no Zn^{2+} affinity, the outer BPA in **NBD-TPEA** should be responsible for the Zn^{2+}-induced photoinduced electron transfer blockage as well as for the enhanced Zn^{2+} binding ability of 4-amine. Successful intracellular Zn^{2+} imaging on living cells with **NBD-TPEA** staining exhibited a preferential accumulation at lysosome and Golgi with dual excitability at either 458 or 488 nm. The intact in vivo Zn^{2+} fluorescence imaging on zebrafish embryo or larva stained with **NBD-TPEA** revealed two zygomorphic luminescent areas around its ventricle which could be related to the Zn^{2+} storage for the zebrafish development. Moreover, high Zn^{2+} concentration in the developing neuromasters of zebrafish can be visualized by confocal fluorescence imaging. This study demonstrates a novel strategy to construct visible light excited Zn^{2+} fluorescent sensor based on ICT fluorophore other than xanthenone analogues. Current data show that **NBD-TPEA** staining can be a reliable approach for the intact in vivo Zn^{2+} imaging of zebrafish larva as well as for the clarification of subcellular distribution of Zn^{2+} in vitro.

Introduction

Zn^{2+} plays vital roles in cellular metabolism, gene expression, apoptosis, neurotransmission, and so forth.[1] It is also associated with physical growth retardation and neurological disorders such as cerebral ischemia and Alzheimer's disease.[2] The spatial and temporal tracking of in vivo Zn^{2+} is challenging but essential to address these issues. Although Zn^{2+} imaging in living cells or hippocampus slices has been achieved using diversified Zn^{2+} sensors,[3,4] intact in vivo Zn^{2+} imaging, which provides information on Zn^{2+} homeostasis and requires a combination of suitable animal models and fluorescent sensors, is highly demanded. The transparent zebrafish embryo or larva is a widely used model in developmental biology, especially for the study of neurode-

[†] School of Chemistry and Chemical Engineering.
[‡] Animal Model Research Center.
[§] Nanjing Xiaozhuang College.

(1) (a) Berg, J. M.; Shi, Y. *Science* **1996**, *271*, 1081–1085. (b) O'Halloran, T. V. *Science* **1993**, *261*, 715–724. (c) Burdette, A. C.; Lippard, S. J. *Proc. Natl. Acad. Sci. U.S.A.* **2003**, *100*, 3605–3610. (d) Frederickson, C. J.; Bush, A. I. *Biometals* **2001**, *14*, 353–366.

(2) (a) Choi, D. W.; Koh, J. Y. *Annu. Rev. Neurosci.* **1998**, *21*, 347–375. (b) Weiss, J. H.; Sensi, S. L.; Koh, J. K. *Trends Pharmacol. Sci.* **2000**, *21*, 395–401. (c) Prasad, A. S. The role of zinc in brain and nerve functions. In *Metals and Oxidative Damage in Neurological Disorders*; Connor, J. R., Ed.; Plenum Press: New York, 1997; Chapter 6, pp 95−111.

(3) (a) Frederickson, C. J.; Kasarskis, E. J.; Ringo, D.; Frederickson, R. E. *J. Neurosci. Methods* **1987**, *20*, 91–103. (b) Nasir, M. S.; Fahrni, C. J.; Suhy, D. A.; Kolodsick, K. J.; Singer, C. P.; O'Halloran, T. V. *J. Biol. Inorg. Chem.* **1999**, *4*, 775–783. (c) Walkup, G. K.; Burdette, S. C.; Lippard, S. J.; Tsien, R. Y. *J. Am. Chem. Soc.* **2000**, *122*, 5644–5645. (d) Sensi, S. L.; Ton-That, D.; Weiss, J. H.; Rothe, A.; Gee, K. R. *Cell Calcium* **2003**, *34*, 281. (e) Hanaoka, K.; Kikuchi, K.; Kojima, H.; Urano, Y.; Nagano, T. *Angew. Chem., Int. Ed.* **2003**, *42*, 2996–2999. (f) Carol, P.; Sreejith, S.; Ajayaghosh, A. *Chem. Asian J.* **2007**, *2*, 338–348. (g) Lim, N. C.; Freake, H. C.; Brückner, C. *Chem.−Eur. J.* **2005**, *11*, 38–49. (h) Kimura, E.; Aoki, S. *Biometals* **2001**, *14*, 191–204. (i) Domaille, D. W.; Que, E. L.; Chang, C. J. *Nat. Chem. Biol.* **2008**, *4*, 168–175. (j) Que, E. L.; Domaille, D. W.; Chang, C. J. *Chem. Rev.* **2008**, *108*, 1517–1549.

(4) (a) Zhang, X.; Lovejoy, K. S.; Jasanoff, A.; Lippard, S. J. *Proc. Natl. Acad. Sci. U.S.A.* **2007**, *104*, 10780–10785. (b) Komatsu, K.; Urano, Y.; Kojima, H.; Nagano, T. *J. Am. Chem. Soc.* **2007**, *129*, 13447–13454. (c) Sumalekshmy, S.; Henary, M. M.; Siegel, N.; Lawson, P. V.; Wu, Y.; Schmidt, K.; Brédas, J.; Perry, J. W.; Fahrni, C. J. *J. Am. Chem. Soc.* **2007**, *129*, 11888–11889. (d) Taki, M.; Wolford, J. L.; O'Halloran, T. V. *J. Am. Chem. Soc.* **2004**, *126*, 712–713.

 10.1021/ja806489y CCC: $40.75

velopment, and its fluorescent imaging has been one of the most frequently used techniques in this field.[5] In fact, the intact in vivo imaging of Ca^{2+} in zebrafish larva has been successfully conducted recently using different Ca^{2+} fluorescent sensors.[6] It is therefore conceivable to use zebrafish larva for in vivo Zn^{2+} fluorescent imaging to clarify the roles of Zn^{2+} in the development of zabrafish, especially in the development of the neurosystem.

For the intact in vivo Zn^{2+} fluorescent imaging of living cells and zebrafish larvae, reduced UV-induced phototoxicity/autofluorescence and sensor-induced interference are essentially demanded.[1c,3c,7] Therefore, visible light excited sensor of biocompatibility is appealing. The reported visible light excited Zn^{2+} fluorescent sensors thus far are mainly derived from bulk xanthenone fluorophores, such as fluorescein and rhodamine.[3c−e,4a,b] Most of them have been successfully applied in cell imaging. However, different laser/filter sets of fluorescence microscopes and the diversified Zn^{2+} imaging experiments, such as the complicated colocalization imaging, require visible light excitable sensors differing in excitation and emission, intracellular distribution, Zn^{2+} binding constants, and so forth.[1c,3b,f−j] Therefore, novel visible light excitable sensors based on fluorophores other than xanthenone are highly desired. Because of the intermolecular charge transfer (ICT) effect, ICT fluorophores with conjugated electron donor (D) and receptor (A) are able to display visible ICT absorption band and large Stokes shift, although their aromatic plane is smaller.[8] In addition to the visible excitability, sensor based on ICT fluorophore may even provide the advantage of lower interference to the living systems because of their small aromatic plane. Moreover, the larger Stokes shift should be favorable for the improvement of imaging quality because of the reduced excitation interference. The possible two-photon excitability of their D$-\pi-$A motif may even offer additional advantage of deeper sectioning in in vivo imaging.[4c] Therefore, the development of novel fluorescent Zn^{2+} sensors based on typical ICT fluorophore is an attractive and promising strategy.

In this work, a novel approach in developing visible light excitable Zn^{2+} fluorescent sensor based on the typical ICT fluorophore, 4-amino-7-nitro-2,1,3-benzoxadiazole (ANBD, $\lambda_{ex} \approx 460$ nm), is reported.[9] The ANBD is closely associated with the frequently used amine labeling agents, 4-chloro- or 4-fluoro-7-nitro-2,1,3-benzoxadiazole (4-ClNBD or 4-FNBD). The two labeling agents emit intensively when their 4-chloro- or 4-fluoro- is substituted by amine to form ANBD fluorophore.[10] More importantly, ANBD derivatives have been frequently affixed to different biomolecules for cell imaging, displaying favorable biocompatibility.[11] Different from the normal photoinduced electron transfer (PET) fluorophores, such as anthracene, this typical ICT fluorophore possesses larger Stokes shift (∼80 nm) and visible absorption band due to the ICT effect from 4-amine to the conjugated 7-NO_2,[9] yet it possesses a smaller aromatic plane. On the other hand, Hg^{2+} sensors, formed by bridging ANBD with sulfur-containing ionophore, displayed not only the emission enhancement but also the emission shift, which demonstrated the possibility to construct a sensor of both PET and photoinduced charge transfer (PCT) sensing behaviors.[12] Since the reported Cu^{2+} sensor 4-bis(pyridin-2-ylmethyl)amino-7-nitro-2,1,3-benzoxadiazole (**NBD-BPA**) with Zn^{2+} ionophore bis(pyridin-2-ylmethyl)amine acting as 4-amino donor group (4-BPA) displayed very poor Zn^{2+} affinity owing to the ICT effect from 4-amine to 7-nitro,[13] in this work, an additional BPA moiety is introduced to replace one of the pyridine of **NBD-BPA** to construct a new Zn^{2+} sensor, **NBD-TPEA**. The additional BPA is expected to coordinate to Zn^{2+} in a synergic manner with the retained (pyridin-2-yl)methylamine (PMA) motif. To clarify the emission and sensing behavior of **NBD-TPEA**, its simple analogue **NBD-PMA** without the outer BPA motif has also been studied for comparison. Chart 1 shows the chemical structures of **NBD-TPEA**, **NBD-PMA**, and **NBD-BPA**.

Chart 1. Chemical Structures of **NBD-TPEA**, **NBD-PMA**, and **NBD-BPA**

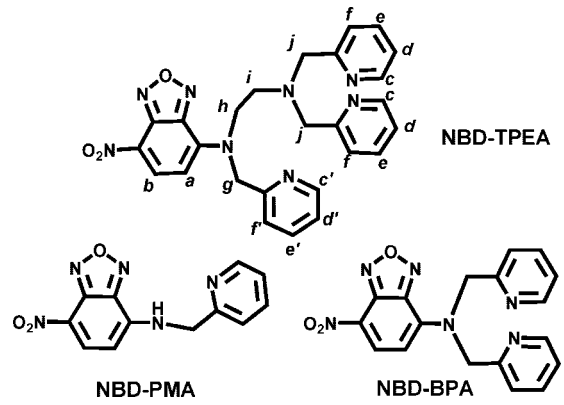

Results and Discussion

Synthesis. NBD-TPEA and **NBD-PMA** were prepared by reacting commercially available 4-ClNBD with *N*,*N*,*N*′-tri(pyridin-2-ylmethyl)ethane-1,2-diamine (TPEA) or PMA in the presence of base in THF. The electron-withdrawing effect of 7-nitro group makes 4-Cl substitutable by nucleophilic agents such as amino- or mercapto- group in ambient condition via an S_N2 pathway. The instant appearance of green emission after

(5) (a) Vogel, G. *Science* **2008**, *322*, 176. (b) Schlosser, G. *Dev. Biol.* **2006**, *294*, 303–351. (c) Grant, K. A.; Raible, D. W.; Piotrowski, T. *Neuron* **2005**, *45*, 69–80. (d) Gilmour, D. T.; Maischein, H.-M.; Nüsslein-Volhard, C. *Neuron* **2002**, *34*, 577–588.
(6) Brustein, E.; Marandi, N.; Kovalchuk, Y.; Drapeau, P.; Konnerth, A. *Pfluegers Arch. Eur. J. Physiol.* **2003**, *446*, 766–773.
(7) Chang, C. J.; Jaworski, J.; Nolan, E. M.; Sheng, M.; Lippard, S. J. *Proc. Natl. Acad. Sci. U.S.A.* **2004**, *101*, 1129–1134.
(8) Grabowski, Z. R.; Rotkiewicz, K. *Chem. Rev.* **2003**, *103*, 3899–4031.
(9) Uchiyama, S.; Santa, T.; Fukushima, T.; Homma, H.; Imai, K. *J. Chem. Soc., Perkin Trans. 2* **1998**, 2165–2173.
(10) (a) Ghosh, P. B.; Whitehouse, M. W. *Biochem. J.* **1968**, *108*, 155–156. (b) Bellon, G.; Malgras, A.; Randoux, A.; Borel, J. P. *J. Chromatogr.* **1983**, *278*, 167. (c) Watanabe, Y.; Imai, K. *Anal. Biochem.* **1981**, *116*, 471–472. (d) Imai, K.; Uzu, S.; Kanda, S. *Anal. Chim. Acta* **1994**, *290*, 3–20. (e) Haugland, R. P.; Spence, M. T. Z.; Johnson, I. D.; Basey, A. *The Handbook: A Guide to Fluorescent Probes and Labeling Technologies*; Molecular Probes: Eugene, OR, 2005; p 1107.
(11) (a) Pagano, R. E.; Sleight, R. G. *Science* **1985**, *229*, 1051–1057. (b) Lipsky, N. G.; Pagano, R. E. *Science* **1985**, *228*, 745–747. (c) Martin, O. C.; Comly, M. E.; Blanchette-Mackie, E. J.; Pentchev, P. G.; Pagano, R. E. *Proc. Natl. Acad. Sci. U.S.A.* **1993**, *90*, 2661–2665. (d) Struck, D. K.; Pagano, R. E. *J. Biol. Chem.* **1980**, *255*, 5404–5410. (e) Kok, J. W.; Eskelinen, S.; Hoekstra, K.; Hoekstra, D. *Proc. Natl. Acad. Sci. U.S.A.* **1989**, *86*, 9896–9900. (f) Gilmanshin, R.; Creutz, C. E.; Tamm, L. K. *Biochemistry* **1994**, *33*, 8225–8232. (g) Leidy, C.; Wolkers, W. F.; Jørgensen, K.; Mouritsen, O. G.; Crowe, J. H. *Biophys. J.* **2001**, *80*, 1819–1828. (h) Rodgers, W.; Glaser, M. *Proc. Natl. Acad. Sci. U.S.A.* **1991**, *88*, 1364–1368.
(12) (a) Sakamoto, H.; Ishikawa, J.; Nakao, S.; Wada, H. *Chem. Commun.* **2000**, 2395–2396. (b) Kim, S. H.; Youn, N. J.; Park, J. Y.; Choi, M. G.; Chang, S.-K. *Bull. Korean Chem. Soc.* **2006**, *27*, 1553–1556.
(13) Banthia, S.; Samanta, A. *New J. Chem.* **2005**, *29*, 1007–1010.

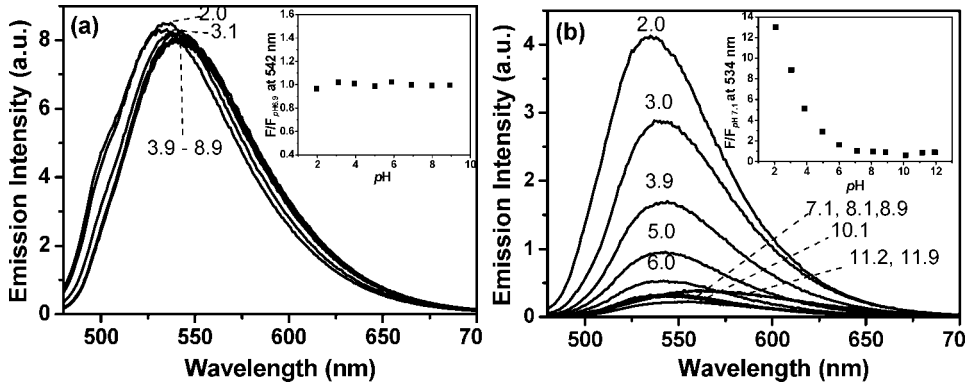

Figure 1. Emission spectra of 5 μM **NBD-PMA** (a) and **NBD-TPEA** (b) in water containing 10% DMSO (v/v) at different pH. $\lambda_{ex} = 469$ nm. The pH value is shown above each individual spectrum. Inset in (a): The fluorescent pH titration profile of **NBD-PMA** according to $F/F_{pH6.9}$ at 542 nm. Inset in (b): The fluorescent pH titration profile of **NBD-TPEA** according to $F/F_{pH7.1}$ at 534 nm.

mixing 4-ClNBD with the amines suggests the reaction is quite efficient. In fact, the nonemissive 4-ClNBD is an effective fluorescent labeling agent for amine-containing compounds in variable chromatographic detection.[10c,d]

Fluorescence of NBD-TPEA and Its pH Dependence. NBD-PMA and **NBD-TPEA** can be readily dissolved in water containing 10% DMSO, and their fluorescence spectroscopic study was carried out in HEPES buffer (pH 7.4) containing 10% DMSO except for the fluorescent pH-dependence determination. For **NBD-PMA**, intensive emission with λ_{ex} and λ_{em} at 469 and 542 nm was observed at neutral condition. This compound displays stable emission at pH 3.9−8.9, whereas the lower pH at 3.1 induces the minor emission blue shift from 542 to 534 nm. The protonation of 4-amine, which is the only amino group in **NBD-PMA**, alters the PCT process, resulting in the blue shift.[14]

However, **NBD-TPEA** fluoresces weakly in neutral aqueous solution (pH 7.4) with λ_{ex} and λ_{em} at 469 and 550 nm, respectively. The Stokes shift of 81 nm satisfies the requirement for a practical sensor providing high quality imaging and is larger than the reported values of many visible light sensors derived from xanthenone analogues (their Stokes shifts are normally ~30 nm). Its emission intensity does not change significantly at pH 7.1−10.1. However, a distinct emission enhancement (enhancement factor of ~13) accompanied by the emission blue shift from 550 to 534 nm can be observed when reducing pH from 7.1 to 2.0 (Figure 1). The stable fluorescence of **NBD-TPEA** at around pH 7.0 is favorable for its in vivo application. In fact, many of the reported visible light excitable Zn^{2+} sensors based on xanthenone structures showed evident fluorescent pH dependence at this condition.[15]

The comparison of the emission behavior between **NBD-PMA** and **NBD-TPEA** reveals that the latter functions mainly as a PET sensor yet possesses some degree of the PCT property.[14] This emission behavior should be attributed to the presence of two amine groups. The BPA (outer amine) connecting to the ANBD fluorophore via an ethylene group is able to quench the emission of ANBD fluorophore via a through-space PET process. However, the 4-amino group (inner amine) functions as the donor of the ICT fluorophore. Both amines can be prontonated at lower pH. At neutral condition, the quantum yield of **NBD-TPEA** accounts for only 1/25 of that of **NBD-PMA** (Figure S1 in the Supporting Information). This should be due to the presence of the additional outer amine group in **NBD-TPEA**, which quenches the emission of ANBD fluorophore via a through-space PET process. The protonation of outer amine at pH ≤ 7.1 blocks the PET process and results in the emission enhancement of **NBD-TPEA**. Moreover, the emission shift of **NBD-TPEA** can be observed at pH 7.4−6 (from 550 to 542 nm) and at pH 3−2 (from 542 to 534 nm). The latter change is identical to the protonation effect of 4-amine observed for **NBD-PMA**. It seems that both 4-amine and pyridine protonation contribute to the emission shift.[13]

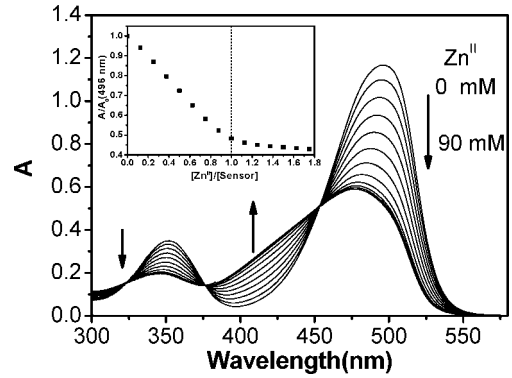

Figure 2. UV spectra of **NBD-TPEA** (40 μM) obtained during the titration by $Zn(NO_3)_2$ (1.5 mM) in HEPES buffer (1:9, DMSO/water, v/v; 50 mM HEPES, 100 mM KNO_3; pH = 7.40). Inset is the titration profile according to the absorbance at 496 nm.

Both **NBD-TPEA** and **NBD-PMA** demonstrate that the 4-amine protonation of ANBD fluorophore only leads to minor blue shift in emission. Therefore, metal coordination at 4-amine in ANBD is not expected to induce large emission shift. This is supported by the fact that the reported Hg^{2+} and Cu^{2+} sensors based on ANBD fluorophore did not show any distinct emission shift in their sensing process.[12,13,16]

Zn^{2+} Binding Behavior of NBD-TPEA. As a Zn^{2+} fluorescent sensor, the Zn^{2+} binding behavior of **NBD-TPEA** was investigated in detail. The UV−vis titration experiment demonstrates that free **NBD-TPEA** has two main absorption bands centering at 496 and 350 nm, which can be assigned to ICT and $\pi-\pi^*$ transition bands, respectively (Figure 2). When Zn^{2+} was added, distinct reduction of the former band can be observed ac-

(14) Jiang, P.; Guo, Z. *Coord. Chem. Rev.* **2004**, *248*, 205–229.
(15) Nolan, E. M.; Ryu, J. W.; Jaworski, J.; Feazell, R. P.; Sheng, M.; Lippard, S. J. *J. Am. Chem. Soc.* **2006**, *128*, 15517–15528.
(16) Boiocchi, M.; Fabbrizzi, L.; Licchelli, M.; Sacchi, D.; Vázquez, M.; Zampa, C. *Chem. Commun.* **2003**, 1812–1813.

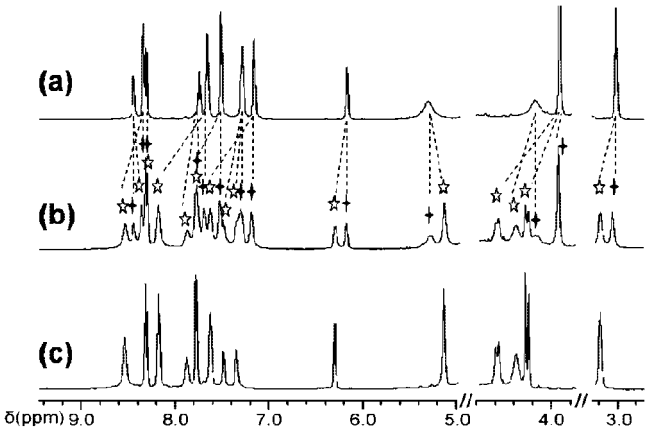

Figure 3. ^{1}H NMR spectra of **NBD-TPEA** obtained during the titration with Zn^{2+} in CD_3OD. (a) Spectrum of free sensor. (b) Spectrum obtained when the ratio of $[Zn^{2+}]_{total}$/[sensor] equals 0.5:1. (c) Spectrum obtained when the ratio of $[Zn^{2+}]_{total}$/[sensor] is 1:1. The signals marked with + and ☆ are for the protons from free sensor and zinc-bound sensor, respectively.

Table 1. Assignments of ^{1}H NMR Spectra of **NBD-TPEA** during Zn^{2+} Titration in CD_3OD

protons	signals for free **NBD-TPEA** (ppm)	signals for Zn^{2+}/**NBD-TPEA** (ppm)
H*c*′	8. 49 (d, 1H, J = 4.0 Hz)	8.37 (s, 1H)
H*c*	8.39 (d, 2H, J = 4.0 Hz)	8.58 (s, 2H)
H*b*	8.35 (d, 1H, J = 9.0 Hz)	8.35 (d, 1H, J = 9.0 Hz)
H*e*′	7.79 (t, 1 H, J = 8.0 Hz)	7.92 (m, 1H)
H*e*	7.70 (t, 2H, J = 7.0 Hz)	8.22 (t, 2H, J = 7.0 Hz)
H*f*	7.55 (d, 2H, J = 7.5 Hz)	7.82 (d, 2H, J = 7.5 Hz)
H*d*′, H*f*′	7.34 (m, 2H)	7.53 (d, 1H, J = 7.5 Hz) H*f*′ 7.39 (m, 1H) H*d*′
H*d*	7.20 (t, 2H, J = 6.0 Hz)	7.67 (m, 2H)
H*a*	6.21 (d 1H, J = 9.0 Hz)	6.34 (d, 1H, J = 9.0 Hz)
H*g*	5.34 (br, 2H)	5.17 (s, 2H)
H*h*	4.20 (br, 2H)	4.42 (s, 2H)
H*j*	3.92 (s, 4H)	4.62, 4.31 (2d, J = 16 Hz)
H*i*	3.06 (t, 2H, J = 6.0 Hz)	3.23 (m, 2H)

companied by the evident hypsochromic shift to 478 nm, suggesting the decreased electron-donating ability of 4-amino group induced by Zn^{2+} binding. Similar change was also observed for the latter band, yet the band shift is much less pronounced. The clear isosbestic points at 453, 375, and 323 nm imply the undoubted conversion of free **NBD-TPEA** to a zinc complex. The titration profile based on the former band shows that the absorbance descends linearly with $[Zn^{2+}]_{total}$ at the $[Zn^{2+}]_{total}$/[**NBD-TPEA**] ratio $\leq$1:1. Higher $[Zn^{2+}]_{total}$ does not lead to any further evident change, suggesting a 1:1 stoichiometry for the zinc complex.

The Zn^{2+} binding behavior of **NBD-TPEA** was further studied by ^{1}H NMR titration in CD_3OD (Figure 3). Upon Zn^{2+} addition, another set of signals for the Zn^{2+}/**NBD-TPEA** complex appears in the spectrum besides the set of signals for free **NBD-TPEA**. When the $[Zn^{2+}]_{total}$/[**NBD-TPEA**] ratio is 0.5:1, two sets of signals display almost identical intensity, wheras when the ratio reaches 1:1, only the signals of zinc complex can be observed. More Zn^{2+} does not lead to any further evident change in the ^{1}H NMR spectrum. The result also confirms that the Zn^{2+} binding ratio of **NBD-TPEA** is 1:1. The detailed assignments of the signals are shown in Table 1. Zn^{2+} coordination triggers a clear downfield shift of H*a* from 6.21 to 6.34 ppm, wheras the signal for H*b* at 8.35 ppm remains unchanged. It suggests that the 4-amino group may be involved in direct Zn^{2+} coordination which decreases the π-electron density of the *meta*-carbon atom. A similar observation was reported by Sakamoto and co-workers in the ANBD-based Hg^{2+} sensor.[12] All the signals for the substituting TPEA undergo significant changes during Zn^{2+} titration process, suggesting that all N atoms of pyridine and amine participate in Zn^{2+} coordination directly. The proposed Zn^{2+} binding mode is shown in Chart 2.

Chart 2. Proposed Zn^{2+} Binding Mode of **NBD-TPEA**

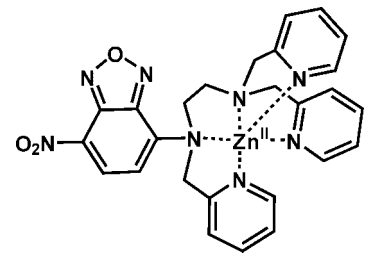

In aqueous medium, **NBD-PMA** does not display any evident change in its UV−vis and ^{1}H NMR spectra when titrated by Zn^{2+}. The results indicate that its 4-PMA motif solely has poor affinity to Zn^{2+}. However, when the additional BPA is introduced to 4-amine via an ethylene bridge in **NBD-TPEA**, the PMA especially its 4-amine is also involved in Zn^{2+} coordination in a synergic manner and alters both the π-electron density and ICT effect of ANBD fluorophore. From the comparison of Zn^{2+} binding behaviors between **NBD-BPA** and **NBD-TPEA**, it can be concluded that the additional outer BPA in **NBD-TPEA** connecting to ANBD via ethylene enhances the Zn^{2+} affinity, whereas the inner BPA (4-BPA) directly connected to NBD ring has poor Zn^{2+} affinity.[13]

Zn^{2+} Fluorescent Response of NBD-TPEA. Fluorescence titration of **NBD-TPEA** by Zn^{2+} in HEPES buffer exhibits a linear emission enhancement with $[Zn^{2+}]_{total}$, and an enhancement factor of ~14 is observed when the $[Zn^{2+}]$/[**NBD-TPEA**] ratio attains 1:1. Then, its fluorescence turns out to be stable and higher $[Zn^{2+}]_{total}$ does not lead to any further evident enhancement, suggesting that there is no additional complex species formed in addition to the 1:1 Zn^{2+}/**NBD-TPEA** complex (Figure 4). As a PET fluorescent compound, the Zn^{2+}-induced emission enhancement of **NBD-TPEA** should mainly be caused by the PET blocking effect induced by the Zn^{2+} coordination to the outer amine. Emission shift from 550 to 534 nm induced by Zn^{2+} addition is similar to that induced by protonation. Therefore, the shift process could be correlated to the Zn^{2+} coordination of 4-amine, which reduces the donating ability of 4-amino group of ANBD. The Zn^{2+}-induced change in ICT effect can be confirmed by the ICT band shift from 496 to 478 nm in UV−vis Zn^{2+} titration.

The Zn^{2+}-specific amplified fluorescence of **NBD-TPEA** was verified by screening against major biologically relevant metal cations. As can be noted from Figure 4b, only Zn^{2+} and Cd^{2+} induce an emission enhancement; all other tested metal cations do not induce any notable emission change. Although Cd^{2+} also induces an emission enhancement, its effect is much less pronounced than that of Zn^{2+} and it will not interfere with Zn^{2+} detection in living cells because of its scarcity. On the other hand, K^+, Na^+, Ca^{2+}, and Mg^{2+}, which are abundant in cells, do not affect Zn^{2+} response even when the [M]/$[Zn^{2+}]$ ratio attains 1000:1. These properties make **NBD-TPEA** a candidate as selective sensor for intracellular Zn^{2+} imaging.

It should be noted that Zn^{2+} binding does not change the excitation maximum of **NBD-TPEA**. The extinction coefficients

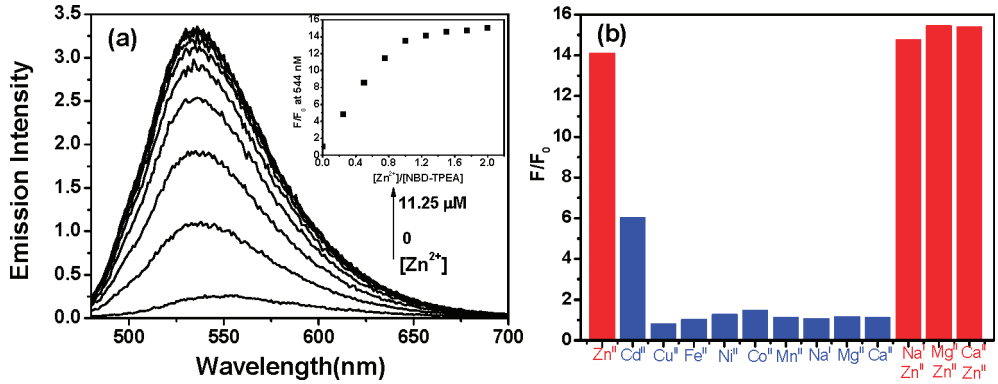

Figure 4. (a) Emission spectra of 5 μM **NBD-TPEA** in HEPES buffer (50 mM HEPES, 0.1 M KNO_3, pH 7.4; DMSO/H_2O, v/v 1:10) titrated by $Zn(NO_3)_2$ (1.25 mM) solution. The $[Zn^{2+}]_{total}$ values in the solution are 0, 1.04, 2.08, 3.13, 4.17, 5.21, 6.25, 7.29, 8.33, and 11.25 μM (from bottom to top). Inset is the titration profile according to F/F_0 at 544 nm. (b) Histogram of F/F_0 at 544 nm induced by 1 equiv of transition-metal cations or 1000 equiv of Na^+, Ca^{2+}, and Mg^{2+} in the same buffer. $\lambda_{Exex} = 469$ nm.

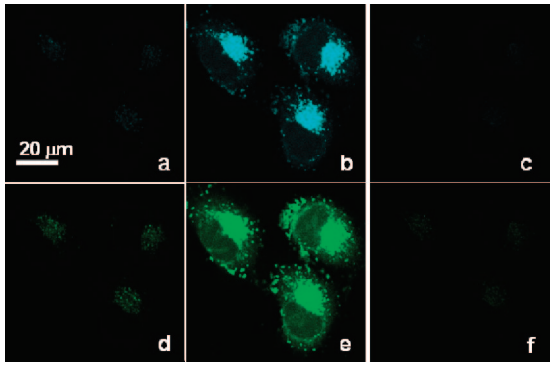

Figure 5. Confocal fluorescence images of HeLa cells upon irradiation at 458 (a,b,c) and 488 nm (d,e,f). (a,d) HeLa cells preincubated in 5 μM **NBD-TPEA** solution at room temperature (20 min). (b,e) Rinsed HeLa cells (1 × PBS, three times) in (a,d) were further incubated in 5 μM $ZnSO_4$/pyrithione (1:1) solution, followed by being rinsed with 5 μM **NBD-TPEA** solution. (c,f) HeLa cells in (b,e) rinsed with 25 μM TPEN solution.

of free **NBD-TPEA** and its zinc complex at excitation maximum are 2.1×10^4 and 1.4×10^4 M^{-1} cm^{-1}, respectively. Their quantum yields in HEPES buffer are 0.003 and 0.046, when determined with *N*-methyl ANBD in acetonitrile as the reference (Supporting Information).[17] The K_d of Zn^{2+}/**NBD-TPEA** complex was determined to be ca. 2 nM from the emission changes of 30 μL of **NBD-TPEA** solution (1 mM) mixed with a series of Zn^{2+}-buffered solutions (Supporting Information).[4d]

Intracellular Zn^{2+} Imaging with NBD-TPEA as Imaging Agent. The intracellular Zn^{2+} imaging ability of **NBD-TPEA** was confirmed first. Since its excitation maximum is 469 nm, both the laser beams of 458 and 488 nm were adopted as excitation light for the confocal imaging (Figure 5). Both excitations give almost identical Zn^{2+} images, and the images under irradiation at 458 nm are obtained at higher output power. Confocal fluorescent imaging of normal HeLa cells stained by **NBD-TPEA** displays a feint luminescent area close to the dim nucleolus. When exogenous Zn^{2+} is introduced into the cells via incubation in $ZnSO_4$/pyrithione solution (5 μM), the former luminescent area becomes brighter and additional scattering bright dots are also observed. When the cells are treated further by membrane-permeable chelator, *N*,*N*,*N*′,*N*′-tetrakis(2-pyridylmethyl)ethylenediamine (TPEN),[3,4] the cells show a recovered dim image with only the former luminescent area displaying even lower brightness. When the focal plane for imaging is changed, scattering bright dots surrounding the dim nucleolus are displayed in the images (Figure S3 in the Supporting Information). The exogenous addition of Zn^{2+} to HeLa cells leads to a sharp emission enhancement. The followed TPEN treatment makes the cells show a recovered image with even lower luminescence. These results indicate that **NBD-TPEA** is an effective intracellular Zn^{2+} imaging agent of cell permeability and visible excitability. Moreover, **NBD-TPEA** may be preferentially accumulated in certain organelles of HeLa cells.

Localization studies of **NBD-TPEA** in HeLa cells were carried out by costaining with lysosome maker Red DND-99, mitochondria marker Red CMXRos (a rhodamine derivative), and Golgi maker BODIPY TR ceramide, respectively (Figure 6).[10e,15] There is no colocalization with Red CMXRos no matter whether with or without exogenous introduction of Zn^{2+}. However, fine colocalization is observed when Red DND-99 is costained with **NBD-TPEA**, and scattered orange dots are observed in the overlaid images. Similary, fine colocalization is also found when BODIPY TR ceramide is costained with **NBD-TPEA** (Figures 6k−o and S4 in the Supporting Information). These results imply that **NBD-TPEA** is preferentially accumulated in lysosome and Golgi apparatus. The successful costaining experiment with mitochondria marker Red CMXRos also suggests that **NBD-TPEA** may be able to function simultaneously with rhodamine-derived Zn^{2+} sensors such as X-RhodZin and RhodZin to track Zn^{2+} in different organelles.[3d] The intracellular Zn^{2+} imaging behaviors of **NBD-TPEA** on other cells such as HepG2, PC12, and A549 were also investigated. Because of the visible excitation, all the imaging displays clear images without apoptosis evidence in the imaging process (Figures S5−S7 in the Supporting Information), while the fluorescence images of HeLa cells dyed by **PBITA** (a UV-excitable Zn^{2+} sensor developed in our laboratory) display evident cell apoptosis and autofluorescence (Figure S8 in the Supporting Information). In fact, the reported intracellular Zn^{2+} imaging with UV-excited sensors such as Zinquin normally gave faint images providing no details in the cells.[18] The intracellular temporal Zn^{2+} tracking ability of the sensor was also investigated on PC12 cells (Figure 7). When dyed by **NBD-TPEA**, the

(17) Uchiyama, S.; Matsumura, Y.; de Silva, A. P.; Iwai, K. *Anal. Chem.* **2003**, *75*, 5926–5935.

(18) (a) Zalewski, P. D.; Forbes, J.; Seamark, R. F.; Borlinghaus, R.; Betts, W. H.; Lincoln, S. F.; Ward, A. D. *Chem. Biol.* **1994**, *1*, 153–161. (b) Zalewski, P. D.; Forbes, I. J.; Betts, W. H. *Biochem. J.* **1993**, *296*, 403–408.

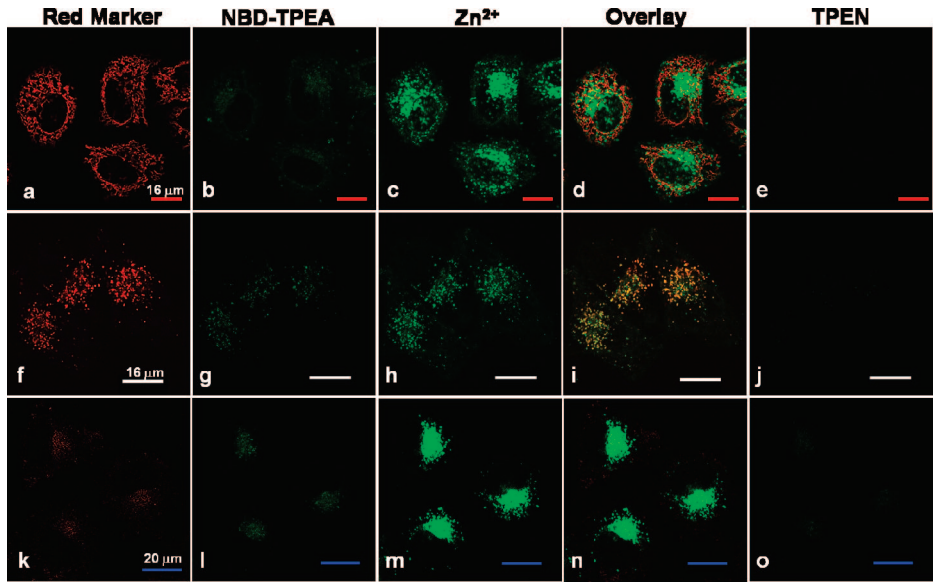

Figure 6. Confocal fluorescence images of HeLa cells preincubated with 50 nM MitoTracker Red CMXRos (or 1 μM LysoTracker Red DND-99, 5 μM BODIPY TR ceramide) and 5 μM **NBD-TPEA**. (a) Fluorescence image visualized by red emission of Red CMXRos, (b) fluorescence image of cells visualized by green emission of **NBD-TPEA**, (c) green fluorescence image of cells after further incubation with 5 μM $ZnSO_4$/pyrithione (1:1) solution, (d) overlay between (a) and (c), (e) green fluorescence image of HeLa cells experienced (c) followed by the treatment with 25 μM TPEN solution, (f) fluorescence image visualized by red emission of Red DND-99, (g) fluorescence image visualized by green emission of **NBD-TPEA**, (h) fluorescence image of cells after incubation with 5 μM $ZnSO_4$/pyrithione (1:1) solution, (i) overlay between (f) and (h), (j) green fluorescence image of HeLa cells experienced (h) followed by the treatment with 25 μM TPEN solution, (k) fluorescence image visualized by BODIPY TR ceramide, (l) fluorescence image of cells visualized by green emission of **NBD-TPEA**, (m) green fluorescence image of cells after incubation with 5 μM $ZnSO_4$/pyrithione (1:1) solution, (n) overlay between (k) and (m), (o) green fluorescence image of HeLa cells experienced (m) followed by the treatment with 25 μM TPEN solution. For the **NBD-TPEA** imaging, irradiation at 488 nm, band path 500−600 nm. For the imaging of Red CMXRos, Red DND-99 and BODIPY TR ceramide, irradiation at 543 nm, band path 555−650 nm.

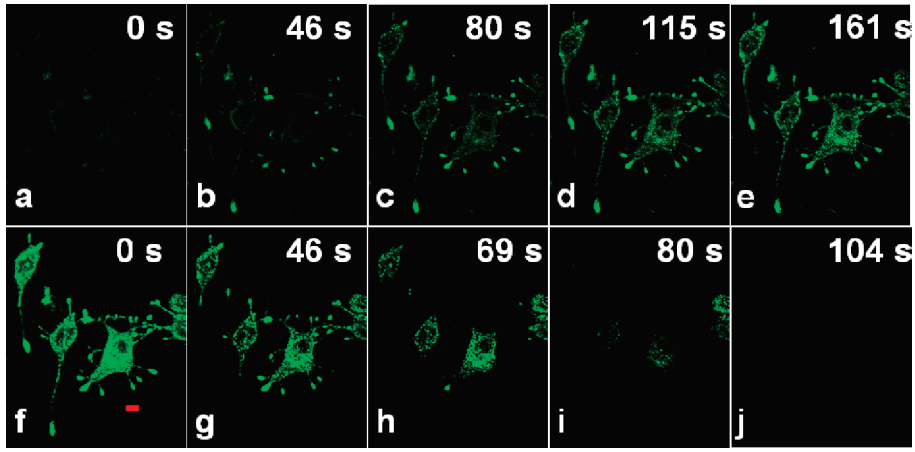

Figure 7. Confocal fluorescence images of PC12 cells preincubated with 5 μM **NBD-TPEA**. (a−e) Fluorescence images in the course of incubation with 5 μM $ZnSO_4$/pyrithione (1:1) solution. (f−j) Fluorescence images of the cells experienced (a−e) obtained in the followed course of the incubation with 25 μM TPEN solution. Red bar = 10 μm.

confocal images display a faint image almost identical to that in Figure 7a. If the cells are further incubated with $ZnSO_4$/pyrithione solution, fast luminescence enhancement can be observed just as shown in Figure 7a−e. The luminescence becomes stable in 5 min, and a bright image similar to that in Figure 7f can be obtained. However, when the cells were further treated with TPEN, the confocal imaging displayed a reverse process and the luminescence disappeared in 104 s. The results suggest that **NBD-TPEA** staining is reversible and **NBD-TPEA** can be an effective sensor for temporal Zn^{2+} tracking.

Intact in Vivo Zn^{2+} Imaging of Zebrafish with NBD-TPEA. The favorable intracellular Zn^{2+} imaging ability on living cells makes the intact in vivo Zn^{2+} imaging on living zebrafish larva conceivable. The preliminary in vivo Zn^{2+} imaging of intact 4-day-old zebrafish larva with **NBD-TPEA** staining was performed first using fluorescence microscope (Figure S9 in the Supporting Information). Although the nonstained zebrafish larva does not exhibit any evident luminescent areas under irradiation, the preincubation of larva with 5 μM **NBD-TPEA** solution at 28.5 °C for 20 min results in two zygomorphic luminescent areas (ZLAs) around its ventricle, accompanied by a few bright dots on the forehead (Figure S9 in the Supporting Information). The development of zebrafish embryo was tracked by **NBD-TPEA** staining. A faint chain composed of green dots close to the bottom of the venter was observed in the initial development stage (Figure 8a). The chain becomes brighter and

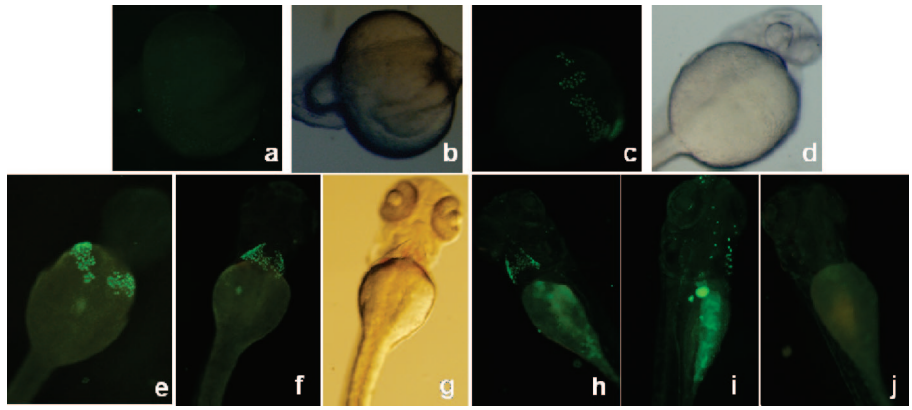

Figure 8. Fluorescence microscopic images of **NBD-TPEA**-stained zebrafish larva incubated at 28.5 °C. 1-Phenyl-2-thiourea (PTU) was added in the incubation media to depress the development of pigment after 8 h of incubation. The final concentration is 0.003%. (a) Fluorescence image of the embryo after 18 h of incubation, (b) bright-field transmission image of (a), (c) fluorescence image after 25 h of incubation, the total length is ~1.9 mm, (d) bright-field image of (c), (e) fluorescence image after 36 h of incubation, the total length is ~2.7 mm, (f) fluorescence image after 54 h of incubation, the total length is ~3.2 mm, (g) bright-field image of (f), (h) fluorescence image of 5-day-old zebrafish larva, the total length is ~3.5 mm, (i) fluorescence image of 7-day-old zebrafish larva, the total length is ~4 mm, (j) fluorescence image of 5-day-old zebrafish larva after being treated by TPEN (1 h, 100 μM).

moves to the upside of the venter after 25 h of incubation. The bright chain moves to the top of the venter after 36 h and becomes necklace-like (Figure 8e). Further incubation makes the necklace move to the zebrafish ventricle, displaying as the ZLAs (Figure 8f, 54 h). There is no evident change in the fluorescent image in the succedent development course. However, the ZLAs are no longer observable in the image of 7-day-old zebrafish, only scattered bright dots are distributed around the ventricle and forehead. The localization of ZLAs with phase contrast image for larva after 48 h of incubation was given also in Figure S10 in the Supporting Information.

The TPEN treatment of 5-day-old larva results in the complete elimination of the ZLAs, suggesting that the ZLAs and the former luminescent necklace should be correlated to the presence of Zn^{2+} (Figure 8j). Inductively coupled plasma mass spectrometry (ICP-MS) data confirm that zinc content in the separated ZLAs of one larva accounts for 74% of the total zinc amount of intact larva (4-day-old), although its volume is less than 1% of the intact larva. Therefore, the disappearance of ZLAs in the later development stages suggests that the ZLAs correspond to the Zn^{2+} storage for the development of zebrafish. Moreover, 12 h incubation of the 4-day-old larva with Zn^{2+}-containing solution (5 μM) induces the numerous bright dots dispersing from the cephalon to venter. Intriguingly, the former ZLAs on the chest are no longer observable. The exact Zn^{2+} feeding effect on the zebrafish development is still unknown (Figure S9c in the Supporting Information).

Compared with the fluorescence image of zebrafish larva stained by **NBPEA-I** (a new visible light excitable Zn^{2+} fluorescent sensor developed in our laboratory), **NBD-TPEA** staining displays images of higher quality because of the lower background fluorescence (Figures S9 and S11 in the Supporting Information). The special in vivo distribution pattern of **NBD-TPEA** in zebrafish larva may contribute to the lower background fluorescence. All the results suggest that **NBD-TPEA** can be used for in vivo Zn^{2+} imaging of zebrafish larva and has the potential to become a useful sensor for clarifying the role of Zn^{2+} in developmental biology.

Confocal fluorescence imaging of the head of Zn^{2+}-fed zebrafish larva (4-day-old) via **NBD-TPEA** staining exhibits symmetrically distributed bright dots between the two eyes (Figure 9). The exact organ of the bright dots is not known yet, but colocalization of the fluorescence and bright-field images

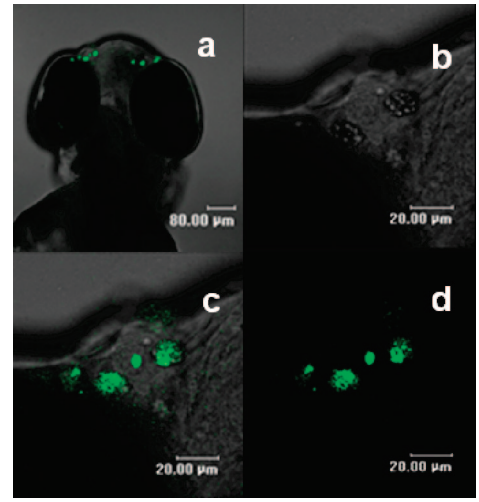

Figure 9. Confocal fluorescence images of the head of a 4-day-old zebrafish larva that was fed in Zn^{2+} solution (5 μM) at 28.5 °C for 12 h. (a) Colocalization of bright-field and fluorescence images for the head (dorsal view). (b) Zoomed bright-field image of the left part of the head. (c) Colocalization of bright-field and fluorescence images for the left part of the head. (d) Zoomed fluorescence image of the left part of the head.

suggests the presence of a high concentration of Zn^{2+}. The position of the bright dots is very close to the neuromasts of the anterior lateral-line system (ALL system) of zebrafish larva that relates to the perception and analysis of the water flow.[5c,19] It is therefore possible to achieve spatial information on Zn^{2+} homeostasis of intact zebrafish embryos via optical sectioning imaging upon **NBD-TPEA** staining. The sensor may also be applied for exploring the neurodevelopment of zebrafish embryos,[5c,d,19] where enriched Zn^{2+} abundance can be easily observed with simple staining procedure.

Conclusions

Novel visible light excited Zn^{2+} fluorescent sensor, **NBD-TPEA**, was designed from small ICT fluorophore, ANBD,

(19) Ghysen, A.; Dambly-Chaudière, C. *Bioessays* **2005**, *27*, 488–494.
(20) (a) Kawabata, E.; Kikuchi, K.; Urano, Y.; Kojima, H.; Odani, A.; Nagano, T. *J. Am. Chem. Soc.* **2005**, *127*, 818–819. (b) Horner, O.; Girerd, J. J.; Philouze, C.; Tchertanov, L. *Inorg. Chim. Acta* **1999**, *290*, 139–144.

utilizing its ICT-induced visible ICT absorption and large Stokes shift. Its distinct selective Zn^{2+}-amplified fluorescence and the Zn^{2+}-induced minor emission shift in aqueous medium can be rationalized and attributed to the synergic Zn^{2+} coordination by its outer amine (BPA) and inner amine, respectively. The sensor displays a selective distribution in lysosome and Golgi as shown from the intracellular Zn^{2+} imaging. In confocal imaging, both 488- and 458-nm laser beams can be used to excite the fluorescence of **NBD-TPEA** effectively, which facilitates its costaining experiments with other dyes. This study demonstrates a novel strategy to construct visible light excitable Zn^{2+} sensors via suitable ICT fluorophore modification, which is different from those based on xanthenone analogues. The smaller aromatic core of **NBD-TPEA** may reduce the sensor-induced interference to the living systems in imaging. Its larger Stokes shift is also helpful for reducing the influence of excitation light. Consequently, **NBD-TPEA** possesses several unique properties including reduced UV-induced interference, dual excitability in confocal imaging, fluorescence pH independence at neutral conditions, and so forth. Intact in vivo Zn^{2+} fluorescence and confocal fluorescence imaging of zebrafish larva with **NBD-TPEA** revealed some interesting phenomena associated with Zn^{2+} distribution, which appears to have never been observed before. Such a sensor could become valuable in revealing the roles of Zn^{2+} in biological systems under either in vitro or in vivo conditions.

Experimental Section

Materials and Methods. 4-ClNBD and PMA were purchased from Aldrich. TPEA was prepared according to the reported procedure.[20] All other reagents were commercially available and of analytical grade. ^{1}H NMR and ^{13}C NMR spectra were determined by a Bruker DRX-500 spectrometer. All the UV−vis spectra were recorded by a Shimadzu UV-3100 spectrophotometer. The emission spectra were obtained using an AMINCO Bowman series 2 fluorescence spectrometer. The pH values of sample solutions were monitored by a PHS-3 system.

Synthesis of NBD-TPEA. 4-ClNBD (907 mg, 4.59 mmol), K_2CO_3 (571 mg, 4.13 mmol), and TPEA (1377 mg, 4.13 mmol) were mixed in 100 mL of THF. The mixture was stirred overnight at room temperature. Then the solids were filtered off and washed with $CHCl_3$. After combining the filtration and the $CHCl_3$ solution, we removed the solvents by evaporation in vacuo. The hygroscopic product was obtained by purifying the resulting mixture with silica gel chromatography. Ethyl acetate/methanol (v/v, 8:1) was used as the eluent. Yield, 63%.

^{1}H NMR (Bruker DRX500, CD_3OD, 500 MHz, δ, ppm): 8.49 (d, 1H, $J = 4.0$ Hz), 8.39 (d, 2H, $J = 4.0$ Hz), 8.35 (d, 1H, $J = 9.0$ Hz), 7.79 (t, 1 H, $J = 8.0$ Hz), 7.70 (t, 2H, $J = 7.0$ Hz), 7.55 (d, 2H, $J = 7.5$ Hz), 7.34 (m, 2H), 7.20 (t, 2H, $J = 6.0$ Hz), 6.21 (d 1H, $J = 9.0$ Hz), 5.34 (br, 2H), 4.20 (br, 2H), 3.92 (s, 4H), 3.06 (t, 2H, $J = 6.0$ Hz). ^{13}C NMR (Bruker DRX500, CD_3OD, 500 MHz, δ, ppm): 160.97, 151.44, 150.59, 147.87, 147.05, 146.89, 139.89, 139.57, 137.64, 126.16, 125.13, 124.79, 124.25, 123.84, 123.82, 104.85 (aromatic C), 62.73, 60.93, 54.56, 52.94 (aliphatic C). Anal. Calcd for $C_{26}H_{24}N_8O_3$: C, 62.89; H, 4.87; N, 22.57%. Found: C, 62.61; H, 5.19; N, 22.30%. ESMS (positive mode, *m*/*z*): 497.2 $[M + H]^+$.

Synthesis of NBD-PMA. PMA (54 mg, 0.5 mmol) and K_2CO_3 (76 mg, 0.55mmol) were mixed in 5 mL of THF, then 4-ClNBD (100 mg, 0.5 mmol) dissolved in 10 mL of THF was added to the mixture dropwise with stirring at room temperature in 0.5 h. The solids were removed via filtration after 3 h. Then the product in the filtrate was purified by silica gel chromatography (dichloromethane/ethyl acetate v/v, 10:1). Yield, 40%.

^{1}H NMR (Bruker DRX-500, CD_3Cl, 500 MHz, δ, ppm): 8.70 (d, 1H, $J = 4.8$ Hz), 8.55 (d, 1H, $J = 8.7$ Hz), 7.97 (b, 1H), 7.80 (t, 1H, $J = 7.9$ Hz), 7.39 (m, 1H), 7.35 (m, 1H), 6.27 (d, $J = 8.4$ Hz), 4.80 (s, 2H). ^{13}C NMR (Bruker DRX-500, CD_3Cl, 500 MHz, δ, ppm): 156.2, 149.2, 147.3, 144.2, 137.9, 137.1, 122.7, 121.6 102.6, 99.9 (aromatic C), 48.2 (aliphatic C). Anal. Calcd for $C_{12}H_9N_5O_3$: C, 53.14; H, 3.34; N, 25.82%. Found: C, 53.43; H, 3.66; N, 25.88%. ESMS (positive mode, *m*/*z*): 272.1 $[M + H]^+$, 294.1 $[M + Na]^+$.

Spectroscopic Study. The emission and excitation spectra of **NBD-TPEA** and **NBD-PMA** (5 μM) were determined in a HEPES buffer (1:9, DMSO/water, v/v; 50 mM HEPES, 100 mM KNO_3; pH = 7.40) using AMINCO Bowman series 2. Its pH dependence of emission was determined in aqueous DMSO solution (5 μM, DMSO/water, 1:9 v/v) at different pH values adjusted by 5 M HNO_3 and 5 M NaOH.

Zn^{2+} Titration of NBD-TPEA and NBD-PMA Solution Determined by UV, Fluorescence, and ^{1}H NMR Spectroscopy. The UV titration experiment of **NBD-TPEA** was carried out by adding aliquots of 10 μL of $Zn(NO_3)_2$ aqueous solution (1.5 mM) to 3 mL of **NBD-TPEA** solution (40 μM, 1:9, DMSO/water v/v; 50 mM HEPES, 100 mM KNO_3; pH = 7.40) in a cuvette. The spectra were recorded after the solution was completely mixed. The fluorescence titration experiment was investigated in a similar procedure. The concentrations of **NBD-TPEA** and $Zn(NO_3)_2$ solutions were 5 μM and 1.25 mM, respectively. Aliquots of 2.5 μL of Zn^{2+} solution were added to 3 mL of **NBD-TPEA** solution (5 μM, 1:9, DMSO/water v/v; 50 mM HEPES, 100 mM KNO_3; pH = 7.40). The excitation wavelength was 469 nm. ^{1}H NMR study of Zn^{2+} titration was carried out on Bruker DRX-500 (500 MHz) at 25 ± 1 °C in CD_3OD. Chemical shift was referenced to an external sample of TMS (δ, 0.00 ppm). The concentration of **NBD-TPEA** was 20 mM, and the concentration of $Zn(NO_3)_2 \cdot 6H_2O$ varied from 0 to 30 mM.

All Zn^{2+} titration experiments of **NBD-PMA** solution were carried out in procedures similar to those described above.

Selective Fluorescent Response of NBD-TPEA to Different Metal Cations. The fluorescent response of **NBD-TPEA** to different metal cations was determined in 5 μM **NBD-TPEA** buffered solution (1:9, DMSO/water, v/v; 50 mM HEPES, 100 mM KNO_3; pH = 7.40). Metal cation solution (12.5 μL, 1.2 mM) was added to 3 mL of this solution, and the fluorescence spectra were determined after complete mixing. The excitation wavelength was 469 nm.

To clarify whether the coexisting alkaline and alkaline earth metal cations affect its Zn^{2+} response, 15 μL of 1 M Ca^{2+}, Mg^{2+}, or Na^+ solution was added following the Zn^{2+} addition (12.5 μL of 1.2 mM $Zn(NO_3)_2$), and the emission was determined after complete mixing. The final concentration of alkaline or alkaline earth metal cation was 1000 times as high as that of Zn^{2+}.

Cell Culture Methods and Staining Procedure. The **NBD-TPEA** working solution for cell staining was prepared from a 5 mM aqueous stock solution (containing 10% DMSO) of **NBD-TPEA** by diluting with 1 × PBS to a final concentration of 5 μM.

HeLa, A549, PC12, and HepG2 cells were cultured in glass bottom dishes following the same procedure. The culture medium was Dulbucco's modified Eagle medium supplemented with 10% fetal bovine serum, 100 units/mL of penicillin, 100 μg/mL of streptomycin, and 3.7 mg/mL of $NaHCO_3$.

For intracellular Zn^{2+} imaging of cells solely stained by **NBD-TPEA**, the incubation media was removed and the cells were rinsed three times with 1 × PBS. Then the cells were incubated in the **NBD-TPEA** working solution for 20 min at room temperature. After removing the solution, we washed the dish three times with PBS. The confocal images of the cells were obtained using a Leica TCS-SL microscope equipped with a 63× oil-immersion objective. The samples were excited at 458 or 488 nm with an Ar laser. A band-pass from 500 to 600 nm was adopted for observation. For intracellular Zn^{2+} imaging of cells with exogenous Zn^{2+}, the exogenous Zn^{2+} was introduced by incubating the cells with 5 μM $ZnSO_4$/2-mercaptopyridine-*N*-oxide solution, which was prepared by diluting 5 mM $ZnSO_4$ and 2-mercaptopyridine-*N*-oxide stock

solutions with 1 × PBS. Then the cells were dyed with **NBD-TPEA** solution in a procedure similar to that described above and imaged.

Zn^{2+} deprival of the **NBD-TPEA** dyed by HeLa cells with exogenous Zn^{2+} by TPEN solution was also investigated. After incubation with 5 μM $ZnSO_4$/2-mercaptopyridine-*N*-oxide solution, the cells were treated with TPEN solution (TPEN stock solution in DMSO was diluted with 1 × PBS and the final concentration was 25 μM) followed by washing with 1 × PBS and then the confocal images were obtained.

For the costaining experiments with **NBD-TPEA** and organelle marker, the PBS-rinsed cells were dyed first by the marker in their individual standard procedure followed by **NBD-TPEA** staining in the procedure described above. Then, the confocal images were obtained respectively at the imaging conditions of the marker or **NBD-TPEA**. After that, the cells were imposed further with exogenous Zn^{2+} in the procedure described above and imaged. Finally, the cells with exogenous Zn^{2+} were deprived with TPEN in the procedure described above. For the lysosome staining by LysoTracker Red DND-99 (from Invitrogen), the HeLa cells were incubated in 1 μM Red DND-99 at room temperature for 5 min, followed by being rinsed with 1 × PBS (two times). For the mitochondria staining with MitoTracker Red CMXRos (Invitrogen), the HeLa cells were incubated in 50 nM of Red CMXRos solution at room temperature for 15 min, followed by being rinsed with 1 × PBS (two times). For the Golgi staining with BODIPY TR ceramide (Invitrogen), the HeLa cells were incubated in 5 μM BODIPY TR ceramide solution at 4 °C for 30 min, then the cells were washed with 1 × PBS two times followed by incubation with 1 × PBS for 30 min. Finally, the cells were washed with 1 × PBS two times before imaging. The excitation wavelength for **NBD-TPEA** in costaining experiments was 488 nm, and the band path was 500−600 nm. The excitation wavelength for LysoTracker Red DND-99, MitoTracker Red CMXRos, and BODIPY TR ceramide was 543 nm. The band path for the marker imaging was from 555 to 650 nm.

Temporal Zn^{2+} tracking was investigated on high differential PC12 cells. Thus, the cells were incubated with 5 μM **NBD-TPEA** solution (5 min) and imaged. After removing the **NBD-TPEA** solution, we added 5 μM $ZnSO_4$/2-mercaptopyridine-*N*-oxide solution and immediately imaged the cells. The imaging lasted for 5 min. Then the Zn^{2+} solution was removed, and 25 μM TPEN solution was added. The imaging was started immediately upon TPEN addition and lasted 5 min.

Intact in Vivo Zn^{2+} Imaging of Zebrafish Larva with NBD-TPEA Staining. Zebrafish embryos or larvae were incubated in pure water from MilliQ system at 28.5 °C. PTU (Sigma) was added into the incubation media to depress the development of pigment after 8 h. The final concentration was 0.003%. The incubation course lasted for more than 7 days. The fluorescence images of the larvae at certain development stage were obtained after incubation with 5 μM **NBD-TPEA** solution at 28.5 °C for 20 min followed by being embedded in methyl cellulose. A Leica MZ16F fluorescence stereomicroscope was adopted for the observation. Light from the mercury lamp through GFP2 filter was used as the excitation light, and the exposure time was 1.0 s. TPEN treatment to zebrafish larvae was also investigated and imaged. The 5-day-old zebrafish larvae were incubated with 25 μM TPEN solution at 28.5 °C after being rinsed with 1 × PBS three times. Then the larvae were washed with PBS three times and dyed by **NBE-TPEA** solution. After being washed by PBS three times, the larvae were also imaged by a fluorescence stereomicroscope in similar conditions.

Four-day-old zebrafish larvae cultured similarly but without PTU were also investigated by fluorescence imaging (Supporting Information). After incubation with 5 μM **NBD-TPEA** solution at 28.5 °C for 20 min, the larvae were washed with 1 × PBS three times and then embedded in methyl cellulose for imaging. The imaging of Zn^{2+}-fed zebrafish larvae was also performed, and non-PTU cultured larvae were used. The 4-day-old zebrafish larvae were fed with 5 μM Zn^{2+} solution at 28.5 °C for 12 h. Then the larvae were washed with 1 × PBS three times followed by **NBD-TPEA** staining in a procedure similar to that described above. Then the larvae were imaged by the fluorescence stereomicroscope in similar conditions. After removing the **NBD-TPEA** solution, we rinsed the Zn^{2+}-fed zebrafish larvae three times with 1 × PBS. Then, the Zn^{2+}-fed zebrafish were incubated further with 25 μM TPEN solution. After removing the TPEN solution and rinsing with PBS three times, we dyed the larvae by **NBD-TPEA** solution and imaged them.

The confocal imaging of 4-day-old Zn^{2+}-fed zebrafish larva (non-PTU cultured) embedded in methyl cellulose was performed on the head with a Leica TCS-SL confocal microscope equipped with a 20× objective at the same conditions given in cell confocal imaging.

ICP-MS Determination of Zinc in Zebrafish Larva and in the Separated Zygomorphic Luminescent Areas Visualized by NBD-TPEA Staining around Its Ventricle. Four-day-old zebrafish larvae were washed with pure water from a Milli-Q system three times, followed by anaesthetization with tricaine. Then every two intact larvae or the separated zygomorphic luminescent areas (separated with microdissecting tweezer under microscope) of three larvae were put respectively into the polyethylene tube (acid-rinsed) filled with 100 μL of pure water. Then all the tubes were added with 50 μL of HNO_3 and incubated at 95 °C for 2 h. After the addition of 20 μL of H_2O_2, the mixtures were incubated at 95 °C for 1.5 h. Finally, 20 μL of HNO_3 was added and the samples were incubated at 37 °C for an additional 0.5 h. After the digestion, the volume of every sample was adjusted to 2 mL with pure water for ICP-MS determination. Zinc analysis was performed with ICP-MS using a standard Plasma-Quad II instrument (VG Elemental, Thermo Optek Corp). The most abundant isotope of zinc (*m*/*z* 65) was measured. Blank samples were also determined as control. $[Zn^{2+}]_{control}$ is 11 ± 2 ppb, $[Zn^{2+}]$ of two intact larva is 20 ± 1 ppb, and $[Zn^{2+}]$ of the separated ZLAs of three larvae is 21 ± 4 ppb. ICP-MS data disclose that zinc content in the separated ZLAs of one larva accounts for 74% of the total zinc amount of intact larva, although its volume is only less than 1% of the intact larva.

Acknowledgment. Financial support from the National Natural Science Foundation of China (Nos. 20571043, 30370351, 90713001, and 20721002) and the Natural Science Foundation of Jiangsu Province (BK2008015) is gratefully acknowledged.

Supporting Information Available: Quantum yield and dissociation constant determination, Figures S1−S11. This material is available free of charge via the Internet at http://pubs.acs.org.

JA806489Y